01 May 2011

Slow Magnetic Relaxation and Electron Delocalization in an S = 9/2 Iron(II/III) Complex with Two Crystallographically Inequivalent Iron Sites

Susanta Hazra

Sujit Sasmal

Michel Fleck

Fernande Grandjean
Missouri University of Science and Technology, grandjeanf@mst.edu

et. al. For a complete list of authors, see https://scholarsmine.mst.edu/chem_facwork/760

Recommended Citation

S. Hazra and S. Sasmal and M. Fleck and F. Grandjean and M. T. Sougrati and M. Ghosh and T. D. Harris and P. Bonville and G. J. Long and S. Mohanta, "Slow Magnetic Relaxation and Electron Delocalization in an S = 9/2 Iron(II/III) Complex with Two Crystallographically Inequivalent Iron Sites," *Journal of Chemical Physics*, vol. 134, no. 17, American Institute of Physics (AIP), May 2011.
The definitive version is available at https://doi.org/10.1063/1.3581028

Slow magnetic relaxation and electron delocalization in an $S = {}^9/_2$ iron(II/III) complex with two crystallographically inequivalent iron sites

Susanta Hazra,[1] Sujit Sasmal,[1] Michel Fleck,[2] Fernande Grandjean,[3] Moulay T. Sougrati,[3] Meenakshi Ghosh,[4] T. David Harris,[5] Pierre Bonville,[6] Gary J. Long,[7,a)] and Sasankasekhar Mohanta[1,a)]

[1]*Department of Chemistry, University of Calcutta, 92 A. P. C. Road, Kolkata 700 009, India*
[2]*Institute for Mineralogy and Crystallography, University of Vienna, Althanstr, 14, A-1090 Vienna, Austria*
[3]*Department of Physics, B5, University of Liège, B-4000 Sart Tilman, Belgium*
[4]*Max-Planck-Institut für Bioanorganische Chemie, Stiftstrasse 34–36, D-45470 Mülheim an der Ruhr, Germany*
[5]*Department of Chemistry, University of California-Berkeley, Berkeley, California 94720, USA*
[6]*CEA-Saclay, Service de Physique de l'Etat Condensé, F-91191 Gif-sur-Yvette, France*
[7]*Department of Chemistry, Missouri University of Science and Technology, University of Missouri, Rolla, Missouri 65409-0010, USA*

(Received 4 February 2011; accepted 30 March 2011; published online 6 May 2011)

The magnetic, electronic, and Mössbauer spectral properties of $[Fe_2L(\mu\text{-}OAc)_2]ClO_4$, **1**, where L is the dianion of the tetraimino-diphenolate macrocyclic ligand, H_2L, indicate that **1** is a class III mixed valence iron(II/III) complex with an electron that is fully delocalized between two crystallographically inequivalent iron sites to yield a $[Fe_2]^V$ cationic configuration with a $S_t = 9/2$ ground state. Fits of the dc magnetic susceptibility between 2 and 300 K and of the isofield variable-temperature magnetization of **1** yield an isotropic magnetic exchange parameter, J, of $-32(2)$ cm^{-1} for an electron transfer parameter, B, of 950 cm^{-1}, a zero-field uniaxial $D_{9/2}$ parameter of $-0.9(1)$ cm^{-1}, and $g = 1.95(5)$. In agreement with the presence of uniaxial magnetic anisotropy, ac susceptibility measurements reveal that **1** is a single-molecule magnet at low temperature with a single molecule magnetic effective relaxation barrier, U_{eff}, of 9.8 cm^{-1}. At 5.25 K the Mössbauer spectra of **1** exhibit two spectral components, assigned to the two crystallographically inequivalent iron sites with a static effective hyperfine field; as the temperature increases from 7 to 310 K, the spectra exhibit increasingly rapid relaxation of the hyperfine field on the iron-57 Larmor precession time of 5×10^{-8} s. A fit of the temperature dependence of the average effective hyperfine field yields $|D_{9/2}| = 0.9$ cm^{-1}. An Arrhenius plot of the logarithm of the relaxation frequency between 5 and 85 K yields a relaxation barrier of 17 cm^{-1}. © *2011 American Institute of Physics*. [doi:10.1063/1.3581028]

I. INTRODUCTION

Over the past two decades, a number of molecules have been shown to retain their magnetization for finite periods of time upon removal of a magnetic field.[1–3] These complexes, which have come to be known as single-molecule magnets, exhibit such slow magnetic relaxation due to a thermal barrier to spin relaxation that arises due to uniaxial anisotropy acting on a high-spin ground state. This barrier is quantified according to the equation $U = S^2|D|$ for integer spins and $U = (S^2 - 1/4)|D|$ for half-integer spins, where S is the ground state spin and D is the axial zero-field splitting parameter. The discovery of single-molecule magnets has generated much interest from a wide range of scientists, as these species could find potential utility in applications such as high-density information storage, quantum computing, and magnetic refrigeration.

While the relaxation barrier of a single-molecule magnet scales with S and D, the strength of magnetic interactions between paramagnetic centers within the molecule must also be considered. The magnitude of these interactions governs how well separated the spin ground state is from excited states. Indeed, mixing of excited states with the ground state spin can lead to a number of fast relaxation pathways, thereby shortcutting the overall anisotropy barrier. To date, the vast majority of single-molecule magnets feature metal centers coupled through a superexchange mechanism, often mediated through oxide[4,5] or cyanide[6] ligands. However, superexchange, especially through multiatom bridges, is often a relatively weak interaction, such that relaxation can be dominated by pathways involving excited states. As an alternative, double exchange[7] via electron delocalization between mixed-valence transition metal ions,[8–11] is generally a much stronger interaction than superexchange, such that the spin ground state is well-isolated even above room temperature. There is a well documented[12,13] example of a spin 9/2 ground state in a class III mixed-valence iron complex but, unfortunately, the relaxation of the magnetization does not slow down in the absence of an applied magnetic field. A more recent example of a spin 5/2 ground state in a class III mixed-valence vanadium complex has been thoroughly investigated.[14] Hence, the synthesis of multinuclear mixed valent iron complexes

a)Authors to whom correspondence should be addressed. Electronic addresses: glong@mst.edu and sm_cu_chem@yahoo.co.in.

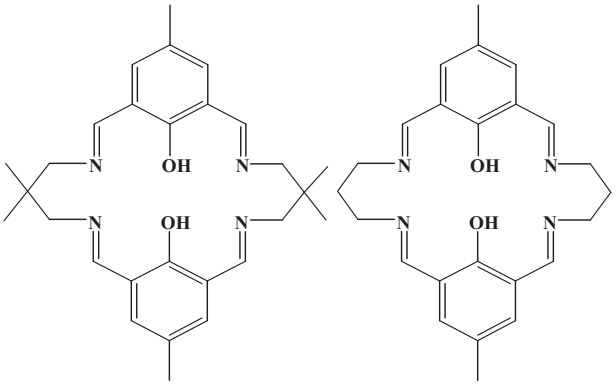

CHART 1. The macrocyclic ligands, H_2L and H_2L^1, used in the preparation of **1**, left, and **2**, right, respectively.

with various ligands is a promising route for the discovery of new complexes exhibiting desirable magnetic properties for applications in fields such as molecular electronics and computing.[15]

Extensive multidisciplinary research into mixed-valence iron complexes has led, through experimental, theoretical, and computational studies,[9–11,16–24] to an enhanced insight into the iron-ligand electron-transfer process and the associated magnetic double exchange mechanism. Further, valence-trapped, class II, and valence-delocalized, class III, mixed-valence iron complexes[8] have been reported in several metalloproteins[25,26] and iron–sulfur proteins.[27–29]

Although several valence-trapped iron(II)-iron(III) complexes have been reported,[17,18] there are only a few examples,[12,13,19] of highly valence-delocalized complexes existing as $Fe^{2.5+}Fe^{2.5+}$ containing complexes, i.e., $[Fe_2]^V$ containing complexes. Only three of these complexes have been characterized by x-ray diffraction, magnetic measurements, and Mössbauer spectroscopy.[12,19] An $S_t = 9/2$ spin ground state has been found in $[(Me_3tacn)Fe(\mu\text{-}OH)_3Fe(Me_3tacn)]_2$, where $Me_3tacn = N, N', N''$-trimethyl-1,4,7-triazacyclononane,[12,13] as shown by the temperature dependence of the molar magnetic susceptibility but, unfortunately, the magnetic relaxation remains too fast at 4.2 K in the absence of an applied magnetic field to observe the magnetic hyperfine splitting in its Mössbauer spectrum. Further, there are only a few complexes exhibiting borderline class II/III behavior.[20] Thus, the design of mixed-valence iron(II)-iron(III) complexes in which the electronic delocalization can be varied from slow to fast, i.e., from valence trapped class II complexes, to partly delocalized class II/III complexes, to completely delocalized class III complexes, is an ongoing challenge.

A fully valence-delocalized $Fe^{2.5+}Fe^{2.5+}$ class III di-iron complex containing two crystallographically *equivalent* iron ions coordinated to the dianionic tetraimino-diphenolate ligand, L^1, see the right portion of Chart 1, has been reported by Nag and co-workers,[19] and it was anticipated that changes in the ligand and, hence, the di-iron coordination environment might yield differing rates of valence-electron delocalization and/or of magnetic relaxation.

By combining synthetic chemistry that yields a new ligand, L, and its associated iron complex, and a microscopic and macroscopic study of its physical properties, we have identified a fully valence-delocalized di-iron complex in which the two iron ions are crystallographically *inequivalent*, with a negative axial zero-field splitting that acts on the $S = {}^9/_2$ ground state to engender slow magnetic relaxation at low temperature. To the best of our knowledge, this complex provides the first example of single-molecule magnetic behavior through double-exchange.

II. EXPERIMENTAL

A. Materials

All the reagents and solvents were purchased from commercial sources and used as received. The mononuclear iron(III) complex, $[Fe(H_2L)(H_2O)Cl](ClO_4)_2 \cdot 2H_2O$, where H_2L is the macrocyclic ligand shown in the left portion of Chart 1, has been prepared by using the method reported[9] earlier, except that 2, 2′-dimethyl-1,3-diaminopropane replaced 1,3-diaminopropane.

B. Synthesis of $[Fe_2L(\mu\text{-}OAc)_2]ClO_4$

$[Fe_2L(\mu\text{-}OAc)_2]ClO_4$, **1**, was synthesized under oxygen-free dry dinitrogen by using standard Schlenk techniques. Solid NaOAc (0.082 g, 1 mmol) and $Fe(ClO_4)_2 \cdot 6H_2O$ (0.063g, 0.25 mmol) were added sequentially to a 25 ml stirred acetonitrile-ethanol (2:3) solution of $[Fe(H_2L)(H_2O)Cl](ClO_4)_2 \cdot 2H_2O$ (0.201 g, 0.25 mmol). After stirring for 2 h, the dark slurry was filtered to remove any suspended particles and the filtrate was cooled to 10 °C a temperature at which a black crystalline precipitate containing diffraction quality single crystals resulted. The crystals were collected by filtration, washed with ethanol, and dried in vacuum. Yield: 148 mg (75%). Anal. Calc. for $Fe_2C_{32}H_{40}N_4O_{10}Cl$: C, 48.79; H, 5.12; N, 7.11. Found: C, 48.70; H, 5.10; N, 7.03. FT-IR (cm^{-1}, KBr): ν(C–H), 2960 w; ν(C = N), 1625 s; $\nu_{as}(CO_2)$, 1557 m; $\nu_s(CO_2)$, 1404 m; $\nu(ClO_4)$, 1088 vs, 622 w.

C. Physical measurements

The C, H, and N elemental analyses were performed with a Perkin-Elmer 2400 II analyzer. The infrared spectra have been recorded between 400 and 4000 cm^{-1} on a Bruker-Optics Alpha-T spectrophotometer in KBr disks. Absorbance spectra were obtained with a Hitachi U-3501 spectrophotometer.

The Mössbauer spectra have been measured between 5.25 and 310 K in a Janis Supervaritemp cryostat with a constant-acceleration spectrometer, which utilized a rhodium matrix cobalt-57 source and was calibrated at 295 K with α-iron powder. The Mössbauer spectral absorbers contained 90 mg/cm^2 of microcrystalline **1** mixed with boron nitride.

Variable-temperature magnetic studies have been carried out with a Quantum Design MPMS SQUID magnetometer. A crystalline powder sample of **1** was placed in a gel capsule and the crystallites were anchored by adding eicosane into the capsule, taking care that the crystallites were well surrounded

by the eicosane. The observed long moments were corrected for the known slightly temperature dependent contribution of the gel capsule and eicosane. A diamagnetic correction of −0.000 350 emu/mol of complex, obtained from tables of Pascal's constants, was applied to the observed molar magnetic susceptibilities. The long moment of **1** has been measured after zero-field cooling to 2 K and subsequent warming to 300 K in a sequence of fields of 0.1, 0.5, 1, and 0.02 T with zero-field cooling between each applied field measurement. The magnetization of **1** was subsequently measured at 2 K between 0 and 7 T. Magnetization data were also collected between 1.8 and 10 K under a range of dc fields. In general, when fitting the magnetization data, several different values of E could be obtained and had little to no effect on the goodness-of-fit, depending only on the input values for E. In addition, often multiple fits of similar quality provided slightly different values of g and D. As such, the average values of these parameters are reported, with the standard deviations given in parentheses. Finally, some fits gave positive values for D, but ac susceptibility measurements demonstrate that D must be negative. Thus, only the magnitude of D was considered when calculating the average value and standard deviation. Ac magnetic susceptibility data have been collected both in a zero dc field between 1.74 and 2.1 K and in a 0.04 mT ac field at frequencies between 1 and 1488 Hz.

Cyclic voltametric measurements have been carried out with a Bioanalytical System EPSILON electrochemical analyzer at a scan rate of 100 mV/s. The concentration of the supporting electrolyte, tetraethylammonium perchlorate, was 0.1 M, whereas that of the complex was 1 mM. The measurements were carried out in acetonitrile solution with a platinum working electrode, a platinum auxiliary electrode, and an aqueous Ag/AgCl reference electrode. The reference electrode was separated from the bulk solution using a tetra- and ethylammonium perchlorate in acetonitrile salt bridge.

D. Crystal structure determination

The single-crystal structure of **1** has been determined at 120 and 293 K with a Nonius Kappa diffractometer equipped with a CCD-area detector, by collecting 641 frames with φ- and ω-increments of one degree with a counting time of 25 s per frame. The crystal-to-detector distance was 30 mm. The reflection data were processed with the Nonius DENZO-SMN[30] programs and corrected for Lorentz polarization, background, and absorption effects. The crystal structure was determined by direct methods, and subsequent Fourier and difference Fourier syntheses, followed by full-matrix least-squares refinements on F^2 using SHELXL-97.[31] All the hydrogen atoms were inserted at calculated positions with isotropic thermal parameters and further refined freely. An anisotropic refinement of the nonhydrogen atoms and an unrestrained isotropic refinement of the hydrogen atoms converged to an R-value of 0.0626 for $I > 2\sigma(I)$ at 120 K. The details of the refinement are given in Tables I and S1 and full details for both the 120 and 293 K structures are given in the crystallographic information files, see the supplementary material.[32]

TABLE I. Crystallographic results for **1**.

Parameter	**1,** 120 K	**1,** 293 K
Empirical formula	$Fe_2C_{32}H_{40}ClN_4O_{10}$	$Fe_2C_{32}H_{40}ClN_4O_{10}$
Formula weight, g/mol	787.83	787.83
Crystal color	Black	Black
Crystal system	Monoclinic	Monoclinic
Space group	$P2/c$	$P2/c$
a, Å	16.094(1)	16.241(3)
b, Å	10.900(1)	11.086(2)
c, Å	21.692(2)	21.795(4)
α, °	90	90
β, °	106.289(3)	105.82(1)
γ, °	90	90
V, Å^3	3652.6(5)	3775.5(9)
Z	4	4
T, K	120(2)	293(3)
2θ	8.30 – 69.90	8.18 – 61.04
μ, mm^{-1}	0.926	0.896
ρ_{calcd}, g cm^{-3}	1.433	1.386
$F(000)$	1636	1636
Scan mode	φ- and ω-scans	φ- and ω-scans
Number of frames	641	641
Scan time per frame, s	25	25
Rotation width, °	1	1
Crystal-detector-dist., mm	30	30
Absorption correction	Multiscan	Multiscan
T_{min}	0.9465	0.9651
T_{max}	0.9552	0.9736
Index ranges	$-25 \le h \le 25$	$-23 \le h \le 23$
	$-17 \le k \le 17$	$-15 \le k \le 15$
	$-34 \le l \le 34$	$-31 \le l \le 31$
Reflections collected	31157	21936
Independent reflections (R_{int})	15974 (0.0263)	11463 (0.0872)
Goodness of fit	1.124	1.005
R_1[a]/wR_2[b] ($I > 2\sigma(I)$)	0.0626/0.1861	0.0804/0.2229
R_1[a]/wR_2[b] (for all data)	0.0858/0.1980	0.2204/0.2850

[a]$R_1 = [\sum||F_o| - |F_c||/\sum|F_o|]$.
[b]w$R_2 = [\sum w(F_o^2 - F_c^2)^2/\sum wF_o^4]^{1/2}$.

III. RESULTS AND DISCUSSION

A. Synthesis and characterization

The $[Fe_2L(\mu\text{-}OAc)_2]ClO_4$, **1**, complex, where L is the dianion of the tetraiminodiphenolate macrocyclic ligand, H_2L, see Chart 1, is readily obtained in high yield from the reaction of $[Fe(H_2L)(H_2O)Cl](ClO_4)_2 \cdot 2H_2O$, $Fe(ClO_4)_2 \cdot 6H_2O$, and NaOAc in a 1:1:4 ratio under a dinitrogen atmosphere. The $\nu_{C=N}$ infrared band in **1** appears at 1625 cm^{-1} and the presence of perchlorate is indicated by the appearance of a very strong absorption at 1088 cm^{-1} and a weak absorption at 622 cm^{-1}. The two medium intensity absorptions observed at 1557 and 1404 cm^{-1} can be assigned to the asymmetric and symmetric stretching modes of the bridging acetate ligands, respectively. The positions of the carboxylate stretching modes indicate that the two acetate ligands bridge the iron ions in the same fashion.[19,33]

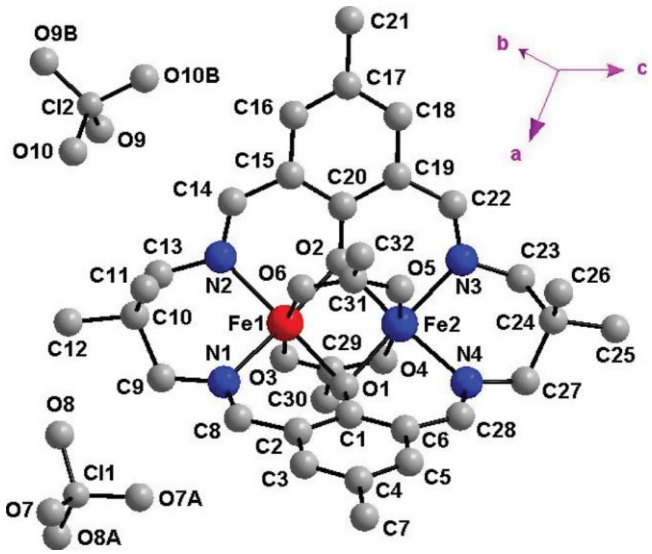

FIG. 1. Crystal structure of $[Fe_2L(\mu\text{-OAc})_2]ClO_4$, **1**. The hydrogen atoms have been omitted for clarity and the two perchlorate anions are each half-occupied.

B. Structure of $[Fe_2L(\mu\text{-OAc})_2]ClO_4$, 1

The crystal structure of **1** is shown in Fig. 1 and selected bond lengths and angles are given in Table II. The structure of **1** reveals a heterobridged bis(μ-phenoxo)bis(μ-acetate) di-iron complex containing the tetraiminodiphenolate macrocyclic dianionic ligand, L^{2-}, and two crystallographically inequivalent iron sites, both of which are hexacoordinated by two azomethine nitrogens, two bridging phenolate oxygens, and the two oxygens from the two bridging acetate ligands. The structure of **1** could not be refined in a higher symmetry group with only one crystallographically unique iron site. Even though, the environment of the two iron sites are similar, as described below, the two sites are crystallographically inequivalent with no symmetry element present that can connect the two sites even if refined in other space groups.

The basal plane of the slightly distorted octahedral coordination environment about the two distinct iron sites in **1** consists of N_2O_2 derived from the L^{2-} ligand; two oxygens from the bridging acetate ligands occupy the axial positions. At 120 K, the average deviations from the least-squares N_2O_2 basal planes about Fe(1) and Fe(2) are $\pm$0.002 and $\pm$0.012 Å, respectively, and Fe(1) and Fe(2) are displaced above the N_2O_2 basal plane by 0.063(3) Å toward O(6) and by 0.068(3) Å toward O(5), respectively.

A comparison of the 120 K bond distances and angles about Fe(1) and Fe(2) in **1**, see Table II, reveals that the two coordination environments are very similar. More specifically, the Fe−O(phenoxo) bond distances of 2.016(2) and 2.023(2) Å for Fe(1) and 2.014(2) and 2.020(2) Å for Fe(2) are the *same* within their statistical errors. In contrast, the Fe−N bond distances of 2.122(2) and 2.127(2) Å for Fe(1) and 2.109(2) and 2.121(2) Å for Fe(2) and the Fe−O(acetate) bond distances of 2.032(2) and 2.079(2) Å for Fe(1) and 2.041(2) and 2.071(2) Å for Fe(2) are somewhat *different* within their statistical errors. These small differences result in a just barely significant difference in the summed bond lengths at the two iron sites, see Tables S2 and S3. Further, the *cisoid* angle range of 83.32° to 99.34° for Fe(1) and 83.87° to 99.51° for Fe(2) and the *transoid* angle range of 170.08° to 175.65° for Fe(1) and 169.30° to 175.31° for Fe(2) are virtually identical. Rather similar conclusions may be reached for the

TABLE II. Bond distances, in Å, and bond angles, in deg, for **1** and a comparison with **2**.

	1, 120 K			**2**, 293 K[a]
Fe(1)–O(3)	2.032(2)	Fe(2)–O(4)	2.041(2)	2.047(2)
Fe(1)–O(6)	2.079(2)	Fe(2)–O(5)	2.071(2)	2.061(2)
Fe(1)–O(1)	2.023(2)	Fe(2)–O(1)	2.020(2)	2.028(2)
Fe(1)–O(2)	2.016(2)	Fe(2)–O(2)	2.014(2)	2.036(2)
Fe(1)–N(1)	2.127(2)	Fe(2)–N(4)	2.121(2)	2.142(2)
Fe(1)–N(2)	2.122(2)	Fe(2)–N(3)	2.109(2)	2.139(2)
Fe(1)–Fe(2)	2.6093(6)			2.7414(8)
O(3)–Fe(1)–O(6)	170.08(7)	O(4)–Fe(2)–O(5)	169.30(7)	165.93(7)
O(1)–Fe(1)–N(2)	175.65(7)	O(1)–Fe(2)–N(3)	175.31(8)	175.45(8)
O(2)–Fe(1)–N(1)	175.23(7)	O(2)–Fe(2)–N(4)	174.28(8)	171.27(8)
O(3)–Fe(1)–O(1)	85.74(7)	O(4)–Fe(2)–O(1)	84.88(7)	87.07(8)
O(3)–Fe(1)–O(2)	86.42(7)	O(4)–Fe(2)–O(2)	86.35(7)	82.85(7)
O(3)–Fe(1)–N(1)	97.50(7)	O(4)–Fe(2)–N(4)	98.52(9)	88.46(8)
O(3)–Fe(1)–N(2)	97.91(8)	O(4)–Fe(2)–N(3)	98.65(8)	97.48(8)
O(6)–Fe(1)–O(1)	87.20(7)	O(5)–Fe(2)–O(1)	87.37(7)	84.59(8)
O(6)–Fe(1)–O(2)	87.87(7)	O(5)–Fe(2)–O(2)	87.67(7)	86.63(8)
O(6)–Fe(1)–N(1)	88.62(7)	O(5)–Fe(2)–N(4)	87.97(8)	102.06(8)
O(6)–Fe(1)–N(2)	89.47(7)	O(5)–Fe(2)–N(3)	89.52(8)	90.93(8)
O(1)–Fe(1)–O(2)	99.34(7)	O(1)–Fe(2)–O(2)	99.51(7)	95.17(6)
O(1)–Fe(1)–N(1)	83.70(7)	O(1)–Fe(2)–N(4)	84.00(8)	85.04(7)
O(2)–Fe(1)–N(2)	83.32(7)	O(2)–Fe(2)–N(3)	83.87(7)	85.31(7)
N(1)–Fe(1)–N(2)	93.43(8)	N(3)–Fe(2)–N(4)	92.39(8)	95.17(8)
Fe(1)–O(1)–Fe(2)	80.39(6)	Fe(1)–O(2)–Fe(2)	80.71(6)	84.83(6)

[a]Data obtained from Dutta *et al.* (Ref. 19).

293 K structure. These structural parameters all indicate that the coordination environments about the two crystallographically distinct Fe(1) and Fe(2) sites are structurally very similar, but, as will be noted below, the differences, especially those observed for the bridging acetate ligands, are enough to lead to two *significantly different* sets of Mössbauer spectral hyperfine parameters for the Fe(1) and Fe(2) sites at 9.1 K and below.

The Fe · · · Fe nonbonding distances of 2.609(1) and 2.601(1) Å observed at 120 and 293 K, respectively, for **1** are shorter than the distance of 2.7414(8) Å observed[19] at 293 K in $[Fe_2L^1(\mu\text{-OAc})_2]ClO_4$, **2**, where L^1 is the dianion of the macrocyclic ligand shown in Chart 1. These Fe · · · Fe nonbonding distances are remarkably short as compared with those observed[22] in the related mixed-valence complexes containing the dianionic L^1 ligand. For example, the Co · · · Co distances[22] in $[Co^{III}Co^{II}L^1Br_2(MeOH)_2]Br_3$ are 3.12(2) and 3.16(1) Å at 283 and 303 K[22] and the Mn · · · Mn distance[22] in $[Mn^{III}Mn^{II}L^1Cl_2Br]$ is 3.168(3) Å at 295(1) K. It should also be noted that at 295 K a very short Fe · · · Fe distance of 2.50(1) or 2.509(6) Å, obtained by EXAFS and single crystal x-ray structural measurements, respectively, has been reported[19] for the fully delocalized $[Fe_2L^2(\mu\text{-OH})_3](ClO_4)_2 \cdot 2MeOH \cdot 2H_2O$, **3**, complex, where L^2 is *N*,*N*′,*N*″-trimethyl-1,4,7-triazacyclononane. Hence, the rather short Fe · · · Fe nonbonding distance of 2.609(1) Å found in **1** at 120 K might well be expected to favor full electron delocalization.

Because the two iron cations in **2** occupy crystallographically equivalent sites, it is highly probable that at least one of the eleven 3*d* electrons is equally shared by the two iron cations and, thus, **2** can be described as a class III $Fe^{2.5+}Fe^{2.5+}$ binuclear complex. In contrast, in **1** the two iron cations occupy crystallographically inequivalent sites, and hence no immediate conclusion can be drawn solely from the structural results about the distribution of the eleven 3*d* electrons between the two crystallographically inequivalent iron cationic sites in **1**. Thus, in order to better understand the electronic properties, we have undertaken a detailed magnetic and Mössbauer spectral study of **1**.

The changes in the crystal structure of **1** between 120 and 293 K are discussed in detail in the supplementary material,[32] where a comparison of the structure of **1** and **2** can also be found.

C. Magnetic properties

The temperature dependences of χ_MT and $1/\chi_M$ of **1** measured in an applied field of 0.02 and 1 T are shown in Fig. 2. The inverse molar magnetic susceptibility, $1/\chi_M$, measured at 0.02, 0.1, 0.5, and 1 T exhibits perfect linear Curie–Weiss law behavior between 2 and 300 K and yields a Curie constant, *C*, of 11.19(6) emu K/mol, a Weiss temperature, θ, of 0.14(25) K, and a corresponding effective magnetic moment, μ_{eff}, of 9.45(3) μ_B per mole; the quoted errors have been obtained from the standard deviation of the parameters obtained at the four applied fields. This perfect linear Curie–Weiss behavior with a very small Weiss temperature indicates

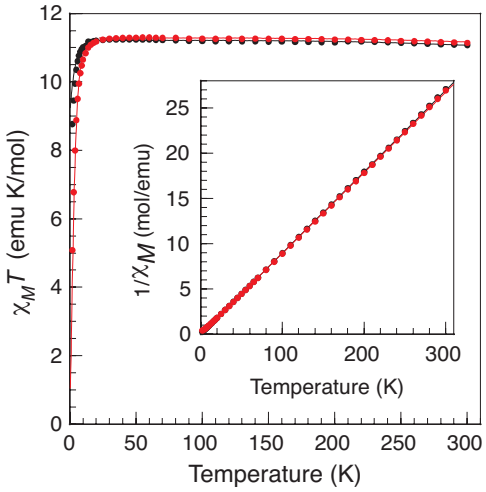

FIG. 2. The temperature dependence of $\chi_M T$ of **1** measured in an applied dc field of 0.02 T, black, and 1 T, red. The black and red solid lines are a fit below 20 K with $g = 1.91$ and 1.92 and $D_{9/2} = -1.04$ and -0.76 cm^{-1}, and between 20 and 300 K with $B = 950$ cm^{-1}, $J = -32(2)$ cm^{-1}, and $g = 1.90(1)$. Inset: The corresponding temperature dependence of $1/\chi_M$ of **1** with a linear Curie-Weiss law fit between 2 and 300 K. The results obtained at 0.02 and 1 T are superimposed upon each other.

an almost perfect paramagnetic behavior and the absence of any long-range magnetic order between 2 and 300 K. The observed μ_{eff} is indicative of a spin 9/2 ground state in full agreement with a fully delocalized electron in a mixed-valence iron(II)-iron(III) binuclear complex.[34] However, the μ_{eff} of 9.45(3) μ_B per mole is smaller than the expected 9.95 μ_B for $S = 9/2$ and corresponds to a *g* value of 1.90(1). At the four applied fields, the product χ_MT in **1** exhibits only a small decrease, from ca. 11.2 to 11.1 emuK/mol, between 20 and 300 K. The decrease in χ_MT below 20 K results from the combined zero-field splitting and Zeeman splitting of the magnetic states and fits of χ_MT with only uniaxial zero-field splitting at applied fields of 0.02, 0.1, 0.5, and 1 T yields $g = 1.91(1)$ and $D_{9/2}$ between -0.76 and -1.04 cm^{-1} or $D_{9/2} = -0.90(14)$ cm^{-1}. In contrast, with the previous magnetic measurements[35,36] on **2**, no cusp was observed at ∼25 K. In order to investigate this apparent difference in the magnetic behavior of **1** and **2**, magnetic susceptibility measurements have been carried out on a sample of **2** anchored in eicosane in an applied field of 0.1 and 1 T, see Fig. S1 in the supplementary material.[32] The cusp previously observed at 25 K in an applied field of 0.5 T was not observed. We conclude that this cusp probably originated either from a poor anchoring of the powder sample or from a paramagnetic impurity.[37]

The analysis of the magnetic susceptibility of **1** and **2** between 20 and 300 K is based on the Hamiltonian for an exchanged-coupled symmetric binuclear complex in the presence of valence delocalization,

$$\boldsymbol{H} = -2J({}^{A}\boldsymbol{S}_A \cdot {}^{A}\boldsymbol{S}_B\mathbf{O}_A + {}^{B}\boldsymbol{S}_A \cdot {}^{B}\boldsymbol{S}_B\mathbf{O}_B) + B\mathbf{T}_{AB}. \quad (1)$$

In the first term, the isotropic Heisenberg exchange term, $\mathbf{O}_A$ and $\mathbf{O}_B$ are the occupation operators and ${}^{A}\boldsymbol{S}_A$ and ${}^{B}\boldsymbol{S}_A$ and ${}^{A}\boldsymbol{S}_B$ and ${}^{B}\boldsymbol{S}_B$ are the spin operators when the transferable electron is on the A or B site, respectively. The second, $B\mathbf{T}_{AB}$, term expresses the mixing of the states $|S_A, S_B, S_{AB})^A$

and $|S_A, S_B, S_{AB}\rangle^B$ where $\mathbf{T}_{AB}$ is the transfer operator, and B is the electron transfer parameter, see the supplementary material.[32] Within this model χ_MT is given by Eq. S3. Both the temperature dependence of the molar magnetic susceptibility, χ_M, and of the product, χ_MT, have been fitted. Because of the known high correlation[35,36] between J and B and the weak temperature dependence of χ_MT between 20 and 300 K, it is virtually impossible to simultaneously determine J and B. In all cases, positive J values lead to poor fits. Additional details concerning the analysis of the temperature dependence of the magnetic susceptibility and the fits are given in the supplementary material,[32] where Tables S4 and S5 summarize the most significant fits. The quoted errors are the statistical errors and the absence of an error indicates that the parameter was constrained to the value given.

It is clear that fits of χ_M and χ_MT lead to similar or insignificantly different results, see Tables S4 and S5. The excellent fits indicate that the iron binuclear complexes in **1** and **2** have a spin 9/2 ground state as expected in the presence of an isotropic antiferromagnetic exchange with a small negative J value and a large electron transfer parameter, B. In other words, the isotropic antiferromagnetic exchange is dominated by the ferromagnetic double exchange. For complex **1** at a fixed $B = 950$ cm^{-1}, $J = -32(2)$ cm^{-1} and $g = 1.91(1)$. For **2** at a fixed $B = 940$ cm^{-1}, $J = -65(5)$ cm^{-1} and $g = 2.02(1)$.

In the fits with fixed J values, the double-exchange parameter, B, was always found to be smaller than 950 cm^{-1}, the value expected from the energy of the intervalence charge transfer band, a reduction that is systematically[14] observed in the analysis of double-exchange mixed valence binuclear complexes and has been attributed to a neglect of vibronic coupling[11,13,38] between the electronic and nuclear motions in the complex. In the case of **1**, there is such a small variation in χ_MT between 20 and 300 K that it is not possible to include this vibronic coupling and fit an additional parameter.

The 2 K magnetization of **1** is shown in the inset to Fig. 3. The absence of saturation and the small magnetization of only 7.38 Nβ at 7 T are indicative of the presence of zero-field

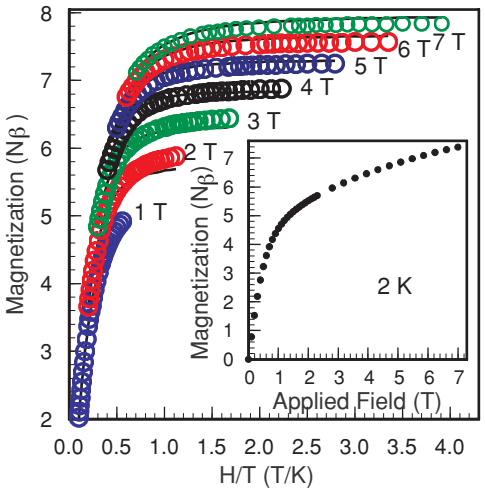

FIG. 3. The low-temperature magnetization of **1** obtained at the indicated applied dc fields. The black lines represent fits of the magnetization. Inset: the dc magnetization of **1** measured at 2 K.

splitting. The effective spin Hamiltonian describing the magnetic anisotropy of the binuclear complex **1** is given by

$$H_{\text{eff}} = D_{9/2}[S_{t,z}^2 - S_t(S_t+1)/3 + E_{9/2}(S_{t,x}^2 - S_{t,y}^2)/D_{9/2}], \quad (2)$$

where $S_t = 9/2$. To further investigate the magnetic anisotropy in **1**, variable-temperature magnetization data have been collected in a range of dc fields. The resulting plot of the reduced magnetization is shown in the main portion of Fig. 3, which reveals the presence of a series of nonsuperimposable isofield curves that are indicative of an anisotropic ground state. To quantify the extent of the zero-field splitting, the magnetization was fit by using ANISOFIT 2.0 (Ref. 39) to obtain the axial and transverse zero-field splitting parameters, $D_{9/2} = -0.89(6)$ cm^{-1} and $|E_{9/2}| = 0.1(1)$ cm^{-1}, respectively, and $g = 1.954(8)$, a g value that agrees rather well with the value of 1.91(1) obtained from the fits of the temperature dependence of χ_M and χ_MT. The anisotropy in **1** likely results from the presence of an orbital contribution to the moment in the complex composed of two iron ions and one delocalized electron. By using the relationship,[12,40] $D_{\text{Fe}} = 2.22D_{9/2}$, between the binuclear complex zero-field splitting parameter and the local zero-field splitting parameters at each iron, one obtains $D_{\text{Fe}} = -2.0(1)$ cm^{-1}, the average local zero-field splitting parameter. In conclusion, the ground state of **1** is characterized by a total spin, $S_t = 9/2$, and in the 10-fold multiplet, whose degeneracy is removed by the crystal field splitting, because $D_{9/2}$ is negative, the $m_t = \pm 9/2$ substate is the ground state. Unfortunately, in the absence of oriented single crystal studies, it is not possible to determine the orientation of the magnetic anisotropy axis.

The observed 0.89(6) cm^{-1} magnitude of $D_{9/2}$ found in **1** is smaller than those observed previously in related binuclear delocalized mixed-valence iron compounds. The previous analyses of the magnetic susceptibility of **2** reported[35,36] $|D_{9/2}| = 1.6$ and 3 cm^{-1}, where the determination of these values may possibly have been affected by the presence of the artificial cusp observed at 25 K. The present analysis of χ_MT of **2** between 2 and 20 K yields $D_{9/2} = -0.70(5)$ cm^{-1} and $g = 2.02$, see Fig. S1. $|D_{9/2}|$ values of 1.8(2) and 1.7 cm^{-1} were observed[12,19] in **3** and $[Fe_2(\mu\text{-}O_2CAr^{Tol})_4(4\text{-}^tBuC_5H_4N)_2]X$, where O_2CAr^{Tol} is 2,6-di(p-tolyl)benzoate and X is PF_6^- or Otf^-, respectively.

Because of the $S = {}^9/_2$ ground state and the negative axial zero-field splitting of $D = -0.89(6)$ cm^{-1} obtained for **1**, the ac magnetic susceptibility of **1** has been measured in order to probe for slow magnetic relaxation. Indeed, variable-frequency ac susceptibility measurements, see Figs. 4 and S2, reveal a strong temperature dependence of both the in-phase, χ_M', and out-of-phase, χ_M'', susceptibilities. Cole–Cole plots of χ_M' vs χ_M'' were then fitted with the generalized Debye model for a solid to obtain the relaxation times at the various temperatures, see Fig. S3.[41] For a single-molecule magnet, the relaxation time, τ, should follow an Arrhenius law, where τ increases exponentially with decreasing temperature. Thus, a plot of $\ln\tau$ vs $1/T$ should be linear, with a slope equal to the energy of the relaxation barrier, U_{eff}. Indeed, such a plot obtained for **1** reveals a linear relationship, see the inset to Fig. 4, and a linear least-squares Arrhenius law fit yields

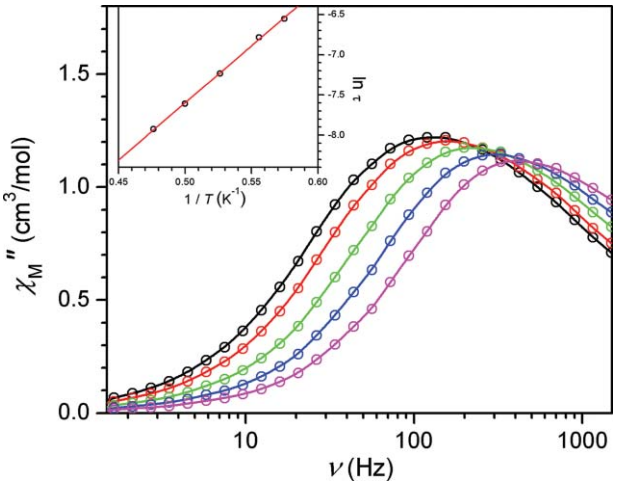

FIG. 4. The variable-frequency out-of-phase ac magnetic susceptibility of **1**, measured at 1.74 K, black, 1.8 K, red, 1.9 K, green, 2.0 K, blue, and 2.1 K, magenta. Inset: An Arrhenius plot of the relaxation time. The solid red line corresponds to a linear fit with $U_{\text{eff}} = 9.8$ cm^{-1}.

$U_{\text{eff}} = 9.8$ cm^{-1} and $\tau_0 = 4.2 \times 10^{-7}$ s. To the best of our knowledge, **1** represents the first example of a single-molecule magnet based on the magnetic behavior of a mixed valence binuclear complex with double-exchange mechanism. The corresponding ac-susceptibility studies for **2** are shown in Fig. S4 and indicate that, because no peak is observed in χ_M'' with increasing frequency between 1.74 and 2.1 K, U_{eff} is too small to be determined at these temperatures. The realization of single-molecule magnetic behavior at more practical temperatures requires a well-isolated spin ground state. Indeed, with exchange constants of $B = 950$ cm^{-1} and $J = -32$ cm^{-1}, the spin ground state of **1** lies ~700 cm^{-1} below the first excited $S = 7/2$ state and could thus support a relaxation barrier well above room temperature if the appropriate bridging ligands can be found to replace the acetate bridging ligands.

All the error bars quoted up to this point are the statistical error bars given by the different fits of the magnetic data. In the presence of a small D value and, hence, of a small orbital contribution to the magnetic moment, a g value slightly larger than 2 is expected for **1**, as is observed for **2**. It is likely that the smaller than 2 values of g obtained from the different fits result from inaccuracies in the mass of the sample, of the gel capsule, and of the eicosane, and in the diamagnetic correction estimated from the Pascal's constants. Although the C, H, and N analysis of **1** is very good and does not point to the presence of an impurity, the presence of a small amount of a diamagnetic impurity cannot be excluded. Hence, the best estimates of the zero-field uniaxial D parameter and g, including experimental inaccuracies, are $-0.9(1)$ cm^{-1} and 1.95(5).

D. Mössbauer spectral study

A detailed iron-57 Mössbauer spectral study of **1** has been undertaken because this spectroscopy probes the microscopic electronic and magnetic properties of each iron in the binuclear complex in the absence of an applied magnetic field and within a timescale of ~5×10^{-8} s, the Larmor precession

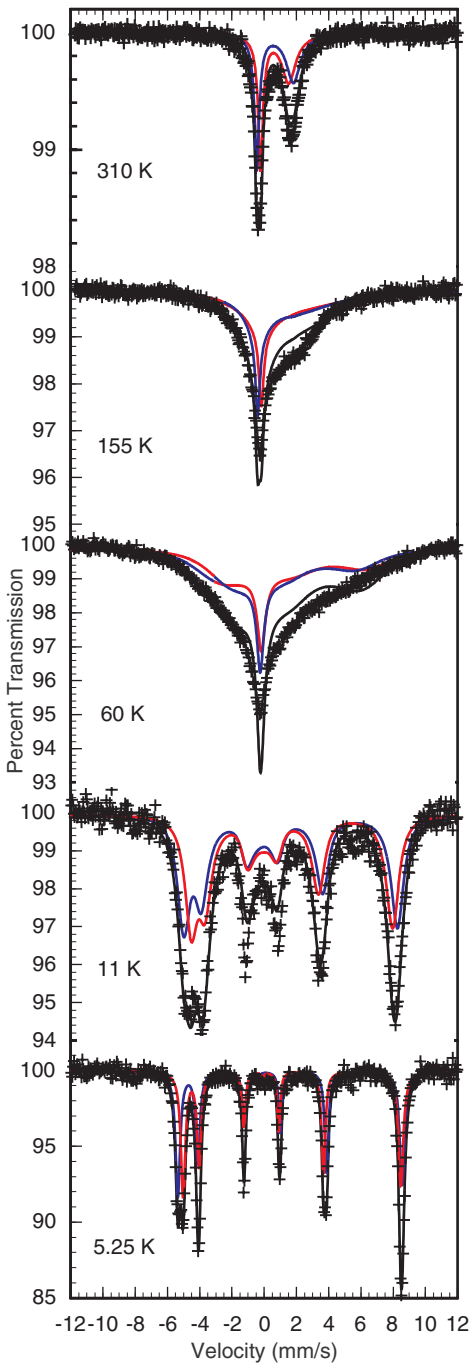

FIG. 5. The iron-57 Mössbauer spectra of **1** obtained at the indicated temperatures. The black solid line is the result of the fit described in the text and the supplementary material (Ref. 32) The red and blue solid lines are the two spectral components in the fit and are tentatively assigned to Fe(1) and Fe(2), respectively.

time of the iron-57 nuclear magnetic moment in the presence of a hyperfine field. The iron-57 Mössbauer spectra of **1** have been measured between 5.25 and 310 K and selected spectra are shown in Figs. 5 and S6.

It is clear from Fig. 5 that at 5.25 K, the Mössbauer spectrum of **1** exhibits two narrow line magnetic sextets, indicating that both iron sites are experiencing a static hyperfine field on the iron-57 Larmor precession time of ~5×10^{-8} s. The 5.25 K spectral parameters are given in Table III. As the tem-

TABLE III. Mössbauer spectral parameters for **1**.[a]

T, K	*Area*[b] (%ε)(mm/s)	Fe site	δ,[c] mm/s	$e^2Qq/2$,[d] mm/s	*H*, T	ν, MHz
310	3.163	2	0.650(5)	1.8	27	514(10)
		1	0.680(5)	2.0	27	514(10)
295	3.611	2	0.660(5)	1.8	27	444(10)
		1	0.690(5)	2.0	27	444(10)
225	7.115	2	0.670(5)	1.8	27	201(5)
		1	0.700(5)	2.0	27	201(5)
155	12.927	2	0.700(5)	1.8	28.5	94.7(5)
		1	0.720(5)	2.0	25.5	94.7(5)
85	23.272	2	0.725(5)	1.8	28	45.3(1)
		1	0.745(5)	2.0	26	45.3(1)
60	28.976	2	0.73(5)	1.8	33	43.5(1)
		1	0.76(5)	2.0	29	43.5(1)
30	33.792	2	0.735(5)	1.8	36	33.7(1)
		1	0.765(5)	2.0	32	33.7(1)
20	35.680	2	0.738	1.8	39.8(1)	22.6(1)
		1	0.768	2.0	32.1(1)	22.6(1)
15	36.606	2	0.74	1.8	40.7(1)	16.7(1)
		1	0.77	2.0	36.8(1)	16.7(1)
11	36.623	2	0.74	1.8	41.1(1)	8.59(5)
		1	0.77	2.0	38.6(1)	8.59(5)
9.1	34.683	2	0.74	1.8	41.3(1)	4.41(5)
		1	0.77	2.0	39.1(1)	4.41(5)
7	35.061	2	0.74	1.8	41.3(1)	1.86(5)
		1	0.76	2.0	39.6(1)	1.86(5)
5.25	36.907	2	0.743(1)	1.816(3)	43.06(1)	0
		1	0.773(1)	2.003(4)	41.68(1)	0

[a]The linewidth was constrained to 0.22 mm/s, the linewidth observed at 5.25 K. Estimated errors are given in parentheses. The absence of an error indicates that the parameter was constrained to the value given.
[b]The statistical error is ± 0.002 (%ε)(mm/s).
[c]The isomer shifts are referred to 295 K α-iron powder.
[d]The asymmetry parameter, η, and the angle, θ, for both sites were found equal to 0.12(2) and 8(2)° at 5.25 K and were constrained to these values at all temperatures. The error bars on η and θ were determined from fits that gave a $\chi^2 = 1.2$ times 1.36, i.e., the best obtained χ^2 shown in Fig. 5.

perature increases the narrow line sextets begin to broaden as is shown in Fig. S6 by the spectra obtained at 7 and 11 K. At 15 and 20 K the Mössbauer spectra of **1** exhibit very broad magnetic sextets. Between 30 and 155 K, the spectra are very broad and exhibit a line shape profile characteristic of a relaxation of the hyperfine field. At 225, 295, and 310 K, the spectra are broad asymmetric doublets that, again, indicate relaxation of the hyperfine field.

The ground state spin 9/2 of **1** observed in the dc magnetic measurements could result either from the presence of one high-spin iron(III) and one high-spin iron(II) ions or from the magnetic double exchange mechanism described in Sec. III C. The isomer shifts of 0.743(1) and 0.773(1) mm/s observed for **1** at 5.25 K are both too high to be assigned to high-spin iron(III) and too low to be assigned to high-spin iron(II) in a pseudooctahedrally coordinated complex, and hence a far more acceptable assignment is to two crystallographically distinct iron ions that experience electron delocalization such that their average valence is 2.5, i.e., a $[Fe_2]^V$ binuclear unit. For comparison, it should be noted that a single isomer shift of 0.841(2) mm/s was observed[19] at 1.8 K for the $[Fe_2L^1(\mu\text{-OAc})_2]ClO_4$, **2**, complex and assigned to a fully valence-delocalized $[Fe_2]^V$ binuclear complex. However, in contrast to the single sextet observed[19] in **2**, two distinct isomer shifts and hyperfine fields are clearly observed and are required to obtain a valid fit of the 5.25 to 11 K spectra of **1**, a requirement that is in full agreement with the two inequivalent iron sites found in its crystallographic structure. Specifically, the different intensities and line widths of the Mössbauer spectral absorptions at -5.5 and $+8.5$ mm/s can only be explained by the use of two sextets. Because the differences in the crystallographic environments of the two iron sites are rather small, fits of the 5.25 K spectrum were attempted with several alternative fitting models including models with a reduced number of adjustable parameters or iron sites. All these alternative fits lead to χ^2 values that are at least twice as large as that of 1.36 shown in Fig. 5; the alternative models are briefly described in the supplementary material.[32]

At this point, it should be noted that these sextets do *not* correspond to long-range magnetic order, an order that is absent as is indicated by the perfectly linear Curie-law behavior observed between 2 and 300 K for the magnetic susceptibility of **1**, see Fig. 2. In contrast, the 5.25 K static hyperfine field results from slow relaxation of the hyperfine field in the $|S_t, m_t> = |9/2, \pm 9/2>$ ground state of **1**. Note that there is no difference in the Mössbauer spectrum for the $m_t = +9/2$ and $m_t = -9/2$ states. The observation[19] of the 4.2 K hyperfine field in **2** results not from the "easy orientation of the internal magnetic field relative to the principal axes of the electric field gradient" as stated in Ref. 19 but from slow

relaxation of the hyperfine field in the same $|S_t, m_t> = |9/2, \pm 9/2>$ ground state, a ground state that is *not* compatible with the earlier reported[36] positive value of $D_{9/2}$. In contrast, in the case of the binuclear complex studied[12] by Ding *et al.*, a complex whose ground state is $|S_t, m_t> = |9/2, \pm 1/2>$, with a positive $D_{9/2}$, no hyperfine field is observed at 4.2 K in the absence of an applied magnetic field. A relaxation path within the electronic multiplet ground state is discussed below.

The hyperfine fields of 43.06(1) and 41.68(1) T observed at 5.25 K in **1** could be characteristic of two high-spin iron(II) ions but are also completely consistent with the presence of two intermediate valence $Fe^{2.5+}$ cations. The assignment to intermediate valence $Fe^{2.5+}$ cations is preferred both in view of the similar hyperfine field of 43.38(1) T reported[19] at 1.8 K for **2** and the magnetic properties discussed in Sec. III C. Similar hyperfine field values of ~47 T have also been observed[12] in related spin 9/2 binuclear complexes and an estimate of their local-spin expectation values has been reported. If the component of the local magnetic hyperfine tensor, A_z, is in the usual range[12,19,42,43] of 16 to 21 T, the observed hyperfine fields indicate that the local-spin expectation values, $\langle S_z \rangle$, are in the range of 2.1 to 2.7. Hence, using the relationship $\langle S_z \rangle = \frac{1}{2}\langle S_{tz} \rangle$, the corresponding total spin expectation value, $\langle S_{tz} \rangle$, for **1** is in the range of 4.2 to 5.4, a range that agrees with its $S_t = 9/2$ ground state.

Finally, the 5.25 K spectrum clearly shows that the quadrupole interactions at the two iron sites in **1** have the same sign and the best fit yields values for $e^2Qq/2$ of 1.816(3) and 2.003(3) mm/s with the same asymmetry parameter, η, of 0.12(2). These $e^2Qq/2$ values are similar to the value of 2.088(4) mm/s reported[19] at 1.8 K for **2** and the values reported for several delocalized di-iron(II/III) compounds.[12,19,38] The angle, θ, between the principal axis of the electric field gradient tensor and the hyperfine field was refined to 8.17(5)° for both sites. The set of fitted hyperfine parameters may not be unique but all the refined values are reasonable and consistent with the observed structure of **1**. Hence, the 5.25 K spectrum presented herein differs essentially from the 1.8 K spectrum obtained for **2** by the presence of two sextets instead of one.[19] As noted above, the magnetically split 5.25 K spectrum does *not* result from long-range magnetic ordering, an ordering that is not observed in the magnetic susceptibility measurements but from slow relaxation of the hyperfine field in the $|S_t, m_t\rangle = |9/2, \pm 9/2\rangle$ ground state. The very narrow line width of 0.220(2) mm/s observed at 5.25 K confirms that there is neither broadening through any relaxation process nor experimental broadening from the spectrometer, which typically yields line widths of 0.23 mm/s for α-iron powder. The assignment of the two sextets to the two iron sites has been tentatively made as described in the supplementary material.[32]

At 7, 9.1, and 11 K, it is also possible to fit the Mössbauer spectra with two sextets with somewhat broadened line widths as a result of the onset of relaxation of the hyperfine field on the Mössbauer time scale of $\sim 5 \times 10^{-8}$ s. The dramatic increase in the spectral line width with increasing temperature above 11 K is equally characteristic of some relaxation of the hyperfine field taking place within the 10-fold multiplet $S = 9/2$ electronic ground state of **1**, the only state to be considered because the $S = 7/2$ multiplet is situated at ~700 cm^{-1} above the ground state.

Electronic relaxation between levels is usually caused by time-fluctuating interactions between the electronic spin and its environment, i.e., with other spins through dipole–dipole coupling, lattice vibrations or phonons coupled to the orbital moment and then to the spin through the spin-orbit interaction. The most likely relaxation mechanism in **1,** studied herein, and in **2,** studied in Ref. 19, should be the intermolecular dipole–dipole interaction and the one phonon, direct, and two-phonon, Raman, processes.[44] In the development of the relaxation interaction in powers of the spin operators, the dominant terms are those in S_+ (or S_-) and ${S_+}^2$ (or ${S_-}^2$), linking states with $\Delta m = \pm 1$ and $\Delta m = \pm 2$, respectively, terms that have an oscillator strength much higher than, for instance, terms in ${S_+}^9$ (or ${S_-}^9$). Hence, the relaxation within the two states of the $|9/2, \pm 1/2\rangle$ doublet is likely to be much faster than within the two states of the $|9/2, \pm 9/2\rangle$ doublet. One can add that "elastic" relaxation between degenerate or quasi-degenerate levels, requiring no energy, is more efficient than "inelastic" relaxation between nondegenerate levels, where the "bath" has to provide the energy difference.

The occurrence and origin of the hyperfine field in paramagnetic binuclear compounds depends on the relative values of the relaxation time or times between the electronic levels, τ_R, and the Mössbauer Larmor precession time, τ_L, ~5 $\times 10^{-8}$ s. In the hypothesis where relaxation is "fast," i.e., $\tau_R << \tau_L$, between all the electronic levels of the binuclear compound, then the hyperfine field is given by

$$H_{\mathrm{hf}}(\mathrm{T}) = A_{\mathrm{hf}}\langle S_z \rangle_{\mathrm{T}} = {}^1\!/_2 A_{\mathrm{hf}}\langle S_{tz} \rangle_{\mathrm{T}},$$

where $\langle S_z \rangle_{\mathrm{T}}$ and $\langle S_{tz} \rangle_{\mathrm{T}}$ are the local and total spin expectation values, respectively, at temperature, T, and A_{hf} is the main component of the magnetic hyperfine coupling tensor. In zero-applied magnetic field at low temperature, where only the electronic ground-state doublet of the binuclear complex is populated, one can then understand the very different 4.2 and 5.25 K spectra observed in Ref. 12 and herein, i.e., a quadrupole doublet-type and a fully developed sharp sextet-type magnetic spectrum, respectively. In Ref. 12, the ground state of the complex is the $|9/2, \pm 1/2\rangle$ doublet, which is degenerate in zero-applied field with $\Delta m = \pm 1$. All the conditions are fulfilled for fast relaxation, and hence, as observed, $H_{\mathrm{hf}} = 0$ because $\langle S_{tz} \rangle = 0$ within this ground-state doublet. In **1**, the ground-state doublet is $|9/2, \pm 9/2\rangle$ and "slow" relaxation within this ground-state doublet is expected because $\Delta m = \pm 9$, and the observed spectrum is due to a "slow relaxation" superposition of hyperfine fields corresponding to $|m_t = +9/2\rangle$ and $|m_t = -9/2\rangle$, which have opposite sign and give identical spectra. Because $\langle S_{tz} \rangle = \pm\, 9/2$ at low temperature, the saturated hyperfine field is given by $H_{\mathrm{hf}} = 9/4\ A_{\mathrm{hf}}$, according to the expression given above.

As temperature increases, in the case of **1** from 5 to 20 K, the excited $|\pm m_t>$ levels, with $|m_t| < 9/2$, gradually become populated and relaxation between different m_t states takes place. A possible relaxation path linking the $|+9/2\rangle$ and $|-9/2\rangle$ states, *via* relaxation mechanisms that allow only $\Delta m = \pm 1$ transitions, is pictured in Fig. 6. "Inelastic" relaxation

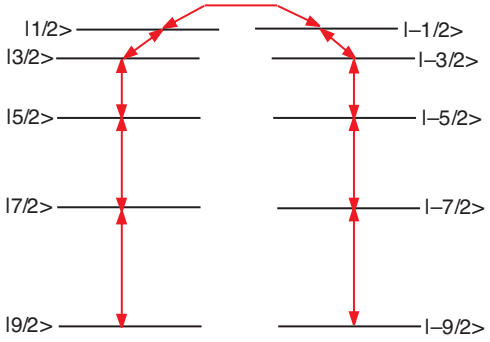

FIG. 6. Possible relaxation path shown as red arrows between the |9/2> and |−9/2> states via excited states within the 10-fold multiplet ground state of **1**.

may occur between the $|9/2\rangle$ and $|7/2\rangle$, $|7/2\rangle$ and $|5/2\rangle$, ... states, but no direct process is allowed between the $|+9/2\rangle$ and the $|-9/2\rangle$ states. Hence, as the temperature increases, rather "fast" relaxation is expected to occur independently between the lowest occupied states of the two "branches" with $m_t > 0$ and $m_t < 0$, a "fast" relaxation that yields a decrease in the observed hyperfine field. A special kind of average over the electronic levels, taking into account that there is "fast" relaxation between the levels in each "branch," but "slow" relaxation between the branches is now introduced and noted by $\langle\langle \ldots \rangle\rangle$. With this notation, $H_{\rm hf}(T) = \frac{1}{2}A_{\rm hf}\langle\langle S_{tz}\rangle\rangle$, where the Boltzmann average is taken over only one of the two "branches". As the temperature increases above 20 K, then the red relaxation path sketched in Fig. 6 may become rather "fast," i.e., the relaxation time between $|9/2\rangle$ and $|-9/2\rangle$, between $|7/2\rangle$ and $|-7/2\rangle$ ... becomes of the order of τ_L and reversal of the hyperfine field occurs, yielding a broadening of the lines and finally a collapse of the magnetic hyperfine structure above 225 K. Of course, the actual situation may be rather more complex, because the crossover between the two regimes with and without hyperfine field reversal is not expected to be well defined and both processes may coexist in a given temperature range. So any fit of the spectra to a relaxation lineshape may be only approximate, but should provide estimates for the average hyperfine field and relaxation time.

The spectra obtained between 5.25 and 310 K have been fitted with a relaxation model[20,44–48] described in the supplementary material[32] and the results of these fits are given in Table III. In the resulting fits shown in Figs. 5 and S6, the effective hyperfine field is reasonably well defined at 60 K and below. Above 60 K, the hyperfine field and the relaxation rate cannot be simultaneously refined because they are highly correlated. Hence, above 60 K, the hyperfine field was kept constant as indicated in Table III. The temperature dependence of the average hyperfine field between 5.25 and 310 K is shown in Fig. 7, where the solid line is the weighted average hyperfine field calculated from the Boltzmann population of the m_t levels of the ground-state 10-fold multiplet for $|D| = 0.9$ cm^{-1} assuming $A_{\rm hf} = 21$ T. The magnitude of the D parameter is in excellent agreement with the range of values between 0.74 and 1.04 cm^{-1} obtained from the dc-magnetic measurements, see above. Above 60 K, the theoretical Boltzmann average predicts a virtually constant hyperfine field of 27 T, as has been used in the fits.

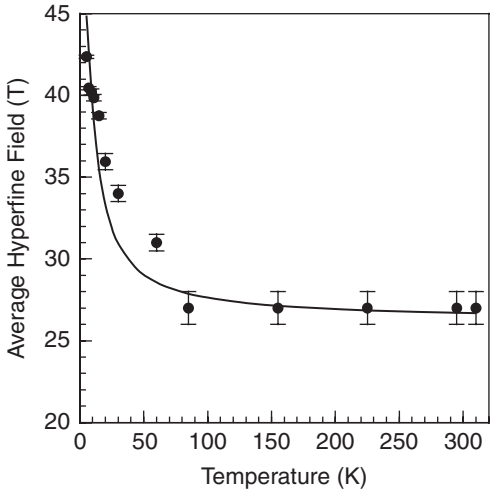

FIG. 7. The temperature dependence of the observed average hyperfine field, circles, and of the average hyperfine field calculated, solid line, for a Boltzmann population of the left or right branch of the $|m_t>$ states shown in Fig. 6.

An Arrhenius plot of the average relaxation frequency in **1** between 5.25 and 310 K is shown in Fig. 8 and a linear fit between 5.25 and 85 K yields an activation energy of 17 cm^{-1}, an energy that is in agreement with the maximum theoretical relaxation barrier of $(S^2 - \frac{1}{4})|D| = 18$ cm^{-1}and the effective energy barrier of 9.8 cm^{-1} for magnetization reversal. Above 155 K, the relaxation process becomes very complex and, as expected, faster because all the m_t sublevels are occupied and provide a fast relaxation pathway.

The temperature dependence of the spectral absorption area of **1** is shown in Fig. S5 and has been fittted with the Debye model[49] for a solid, a model that is perhaps a rather oversimplified approximation for **1**. The resulting Debye temperature, Θ_D, is 125(1) K, a value that is similar to those observed[50] in other organometallic and coordination complexes. The value observed for **1** is relatively small and clearly indicates a soft crystalline lattice that will easily couple to the spin system to provide vibrational energy. The temperature

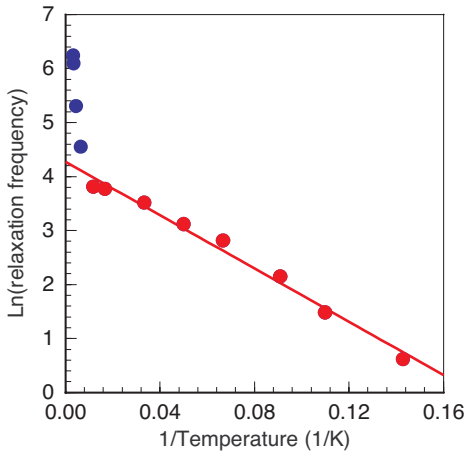

FIG. 8. An Arrhenius plot of the logarthim of the relaxation frequency in **1**, where the red and blue points correspond to low and high temperature regimes.

dependence of the average isomer shift in **1** is shown in Fig. S7 and discussed in the supplementary material.[32]

E. Electronic spectra

The electronic spectrum of **1** measured at 295 K exhibits both a sharp absorption at 353 nm with $\varepsilon = 13\,120\ M^{-1}cm^{-1}$, an absorption that arises from an intraligand transition and a shoulder at 430 nm with $\varepsilon = 6530\ M^{-1}cm^{-1}$, an absorption that arises from a phenolate to iron ion charge transfer transition.

An intense absorption is also observed in **1** at 1053 nm with $\varepsilon = 850\ M^{-1}cm^{-1}$, an absorption that arises from an intervalent charge transfer transition, see Fig. 9. It should be noted that in **2** this absorption is observed[19] at 1060 nm and is more intense with $\varepsilon = 1250\ M^{-1}cm^{-1}$. In contrast, both the 758 nm position and the $\varepsilon = 2400\ M^{-1}cm^{-1}$ intensity of the intervalent charge transfer absorption in **3** is significantly different from those observed in **1** and **2**.[19] The intervalent charge transfer absorption observed in **1** has been measured in several noncoordinating solvents such as chloroform, dichloromethane, and nitrobenzene. In all these noncoordinating solvents the position, intensity, and line width at half-maximum, $\Delta\nu_{1/2}$, are virtually identical, see the upper absorption lines in Fig. 9. Both this noncoordinating, solvent independent, spectral behavior and the observation that the experimental $\Delta\nu_{1/2}$ of 3263 cm^{-1} is much smaller than the $\Delta\nu_{1/2} = 4684\ cm^{-1}$ line width predicted by Hush, confirm that complex **1** is a fully electron delocalized class III complex.[8,9,11,19] Although the intervalent charge transfer absorptions observed for **1** in acetonitrile and acetone are similar to those observed in noncoordinating solvents, in coordinating solvents such as DMF or DMSO the spectral profile has changed because of solvolysis, see the lower lines in Fig. 9.

Clearly, complex **1** remains fully delocalized both in noncoordinating solvents and in acetonitrile and acetone. The degree of electron coupling, H_{AB}, in delocalized complexes is given by $1/2\nu_{max} = 4748\ cm^{-1}$, where ν_{max} is the energy of the intervalent charge transfer absorption band. Further, because $\nu_{max} = 10B$, where B is the double exchange parameter,[12,19] $B = 950\ cm^{-1}$ for **1**. A similar influence of the solvent on the intervalent charge transfer absorption has also been observed for **2**.[19] In the case of **2**, the experimental $\Delta\nu_{1/2}$ is 3980 cm^{-1}, the predicted $\Delta\nu_{1/2}$ is 4668 cm^{-1}, H_{AB} is 4717 cm^{-1}, and B is 943 cm^{-1}.

Although the spectra of **1** and **2** indicate that they are both valence-delocalized even in solution, the $\Delta\nu_{1/2}$, H_{AB}, and B values indicate that the extent of delocalization is slightly greater in **1** than in **2**. For the valence-delocalized complex **3**, the B and H_{AB} values obtained from an electronic spectral study are 1319 cm^{-1} and 6596 cm^{-1}, respectively.[19] It is relevant to mention that for **3** the $B = 1300\ cm^{-1}$ value obtained from a Mössbauer spectral analysis is almost identical to the 1319 cm^{-1} value obtained from the electronic spectral study.[12]

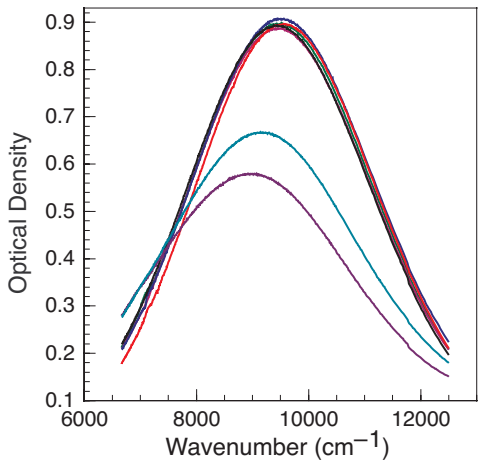

FIG. 9. Intervalent charge transfer absorption band in **1** measured in chloroform, blue; dichloromethane, red; nitrobenzene, black; acetone, green; acetonitrile, magenta; dimethylformamide, cyan; and dimethylsulfoxide, purple. The first five solvents lead to very similar absorption bands.

F. Electrochemical studies

The cyclic voltametric measurements of complex **1** have been carried out in acetonitrile at 298 K in a dinitrogen atmosphere by using platinum as the working electrode. The cyclic voltamogram, obtained between potentials of 0.9 and −0.5 V, is shown in Fig. 10. The one electron reduction $[Fe_2]^{V} \rightarrow Fe^{II}Fe^{II}$ takes place quasi-reversibly at $E_{1/2} = -0.19$ V with $\Delta E_p = 105$ mV, but, in contrast, the oxidation at $E_{p,a} = 0.70$ V is irreversible. It may be noted that in the cathodic sweep a weak peak is observed at 0.20 V. When the cyclic voltametric measurements are carried out between 0.3 and −0.5 V, prior to the $[Fe_2]^{V} \rightarrow Fe^{II}Fe^{II}$ reduction at −0.19 V no electrochemical response is observed at 0.20 V, see Fig. S8. In contrast, as is shown in Fig. S9, this wave appears when the measurement is carried out between 0.0 and 1.0 V. Clearly in **1**, following the oxidation of $[Fe_2]^{V}$ to $Fe^{III}Fe^{III}$, a chemical reaction occurs. It is logical to conclude that the iron(III) containing $[Fe_2L(\mu\text{-}OAc)_2]^{2+}$ moiety generated will be highly unstable because of the very close proximity of the two iron(III) ions and, as a result of coulombic repulsion, one of the iron(III) ions will be detached from the macrocyclic ring and the species that remains is then reduced at 0.20 V.

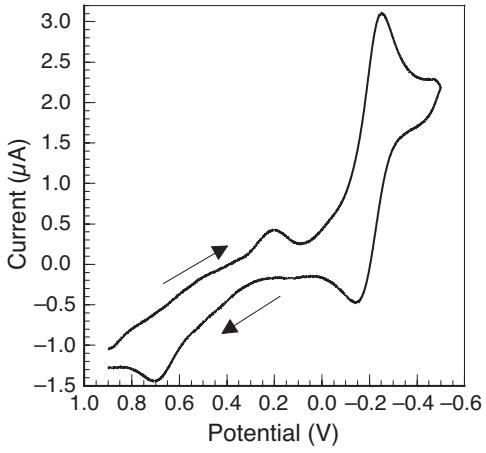

FIG. 10. Cyclic voltamogram of **1** measured in acetonitrile.

IV. CONCLUSIONS

To the best of our knowledge, $[Fe_2L(\mu\text{-}OAc)_2]ClO_4$, **1**, is the first example of a fully valence-delocalized $Fe^{2.5+}Fe^{2.5+}$ or $[Fe_2]^V$ binuclear complex in which the electron delocalization takes place between two crystallographically *inequivalent* iron sites. Further, **1** exhibits both a spin 9/2 ground state as a consequence of double exchange and single molecule magnetic behavior in agreement with a negative axial zero-field splitting parameter.

Although from the aspect of connectivity and chemical bonding the two iron sites in **1** seem rather similar, they must be crystallographically inequivalent because there is no symmetry operation that connects the two iron sites. Further, the coordination environments at the two iron cations are sufficiently different that the two sites exhibit significantly different Mössbauer-spectral hyperfine parameters, albeit parameters that are characteristic of a class III fully electron-delocalized mixed valence $[Fe_2]^V$ complex. Between 5.25 and 11 K the two spectral components exhibit slightly different isomer shifts and different quadrupole interactions and hyperfine fields; both sets of parameters are intermediate between those expected of high-spin iron(II) and high-spin iron(III) ions.

The absorption spectrum of **1** exhibits a strong intervalence charge transfer band at 1053 nm, a band that corresponds to an electron transfer parameter, B, of 950 cm^{-1}.

The magnetic properties indicate that **1** is paramagnetic with an $S = 9/2$ ground state, a spin-state that results from a combination of magnetic double exchange coupling through electron delocalization in the $[Fe_2]^V$ binuclear complex. The analysis, between 2 and 300 K, of the ensemble of magnetic properties of **1**, i.e., the temperature dependence of the dc-magnetic susceptibility, the low-temperature field dependence of the dc magnetization, and the variable-frequency ac magnetic susceptibility, yields the following parameters, including the experimental inaccuracies, an isotropic exchange coupling parameter, J, of $-32(2)$ cm^{-1} for a double-exchange parameter, B, of 950 cm^{-1}, a uniaxial zero-field parameter, $D_{9/2}$, of $-0.9(1)$ cm^{-1}, a rhombic zero-field parameter, $|E_{9/2}|$, of $0.1(1)$ cm^{-1}, and $g = 1.95(5)$, and an effective magnetic relaxation barrier, U_{eff}, of 9.8 cm^{-1} and an attempt time of relaxation, τ_0, of 4.2×10^{-7} s.

The analysis of the temperature dependence of the average hyperfine field between 5.25 and 30 K yields a $|D_{9/2}| = 0.9$ cm^{-1} in excellent agreement with the magnetic measurements and the analysis of the relaxation frequency of the hyperfine field between 5.25 and 85 K yields an activation energy of 17 cm^{-1}. In view of the D value, a maximum theoretical relaxation barrier of $(S^2 - 1/4)|D| = 18$ cm^{-1} is expected. Hence, both magnetic and Mössbauer spectral measurements give reasonable estimates of the relaxation barrier of the spin 9/2 binuclear complex.

ACKNOWLEDGMENTS

The authors thank Professor J. R. Long for the use of the SQUID magnetometer, Professor Charles E. Johnson for helpful discussions during the course of this work, and Dr. R. P. Hermann for help with some programming code. Financial support from the Government of India through the Department of Science and Technology (grants SR/S1/IC-12/2008), the Council for Scientific and Industrial Research for a fellowship to S.H., the University Grants Commission for a Fellowship to S.S., and the Fonds National de la Recherche Scientifique, Belgium (grants 9.456595 and 1.5.064.05) is gratefully acknowledged.

[1] R. Sessoli, H. L. Tsai, A. R. Schake, S. Wang, J. B. Vincent, K. Folting, D. Gatteschi, G. Christou, and D. N. Hendrickson, J. Am. Chem. Soc. **115**, 1804 (1993); R. Sessoli, D. Gatteschi, A. Caneschi, and M. A. Novak, Nature (London) **365**, 141(1993); C. P. Berlinguette, D. Vaughn, C. Cañada-Vilalta, J. R. Galán-Mascarós, and K. R. Dunbar, Angew. Chem., Int. Ed. **42**, 1523 (2003); E. J. Schelter, A. V. Prosvirin, and K. R. Dunbar, J. Am. Chem. Soc. **126**, 15004 (2004).

[2] Y. Song, P. Zhang, X.-M. Ren, X.-F. Shen, Y.-Z. Li, and X.-Z. You, J. Am. Chem. Soc. **127**, 3708 (2005); J. H. Lim, J. H. Yoon, H. C. Kim, and C. S. Hong, Angew. Chem., Int. Ed. **45**, 7424 (2006); C. J. Milios, A. Vinslava, W. Wernsdorfer, S. Moggach, S. Parsons, S. P. Perlepes, G. Christou, and E. K. Brechin, J. Am. Chem. Soc. **129**, 2754 (2007).

[3] C.-F. Wang, J.-L. Zuo, B. M. Bartlett, Y. Song, J. R. Long, and X.-Z. You, J. Am. Chem. Soc. **128**, 7162 (2006); D. E. Freedman, D. M. Jenkins, A. T. Iavarone, and J. R. Long, J. Am. Chem. Soc. **130**, 2884 (2008); D. Yoshihara, S. Karasawa, and N. Koga, J. Am. Chem. Soc. **130**, 10460 (2008); P.-H. Lin, T. J. Burchell, L. Ungur, L. F. Chibotaru, W. Wernsdorfer, and M. Murugesu, Angew. Chem., Int. Ed. **48**, 9489 (2009).

[4] S. L. Castro, Z. Sun, C. M. Grant, J. C. Bollinger, D. N. Hendrickson, and G. Christou, J. Am. Chem. Soc. **120**, 2365 (1998); S. M. J. Aubin, N. R. Dilley, L. Pardi, J. Krzystek, M. W. Wemple, L.-C. Brunel, M. B. Maple, G. Christou, and D. N. Hendrickson, J. Am. Chem. Soc. **120**, 4991 (1998); A. L. Barra, A. Caneschi, A. Cornia, F. Fabrizi de Biani, D. Gatteschi, C. Sangregorio, R. Sessoli, and L. Sorace, J. Am. Chem. Soc. **121**, 5302 (1999); E. M. Rumberger, S. J. Shah, C. C. Beedle, L. N. Zakharov, A. L. Rheingold, and D. N. Hendrickson, Inorg. Chem. **44**, 2742 (2005).

[5] H. Oshio, N. Hoshino, T. Ito, and M. Nakano, J. Am. Chem. Soc. **126**, 8805 (2005); S. Maheswaran, G. Chastanet, S. J. Teat, T. Mallah, R. Sessoli, W. Wernsdorfer, and R. E. P. Winpenny, Angew. Chem., Int. Ed. **44**, 5044 (2005); N. E. Chakov, S.-C. Lee, A. G. Harter, P. L. Kuhns, A. P. Reyes, S. O. Hill, N. S. Dalal, W. Wernsdorfer, K. A. Abboud, and G. Christou, J. Am. Chem. Soc. **128**, 6975 (2006); C. Lampropoulos, G. Redler, S. Data, K. A. Abboud, S. Hill, and G. Christou, Inorg. Chem. **49**, 1325 (2010).

[6] M. Ferbinteanu, H. Miyasaka, W. Wernsdorfer, K. Nakata, K. Sugiura, M. Yamashita, C. Coulon, and R. Clérac, J. Am. Chem. Soc. **127**, 3090 (2005); D. Li, S. Parkin, G. Wang, G. T. Yee, A. V. Prosvirin, and S. M. Holmes, Inorg. Chem. **44**, 4903 (2005); H. Miyasaka, H. Takahashi, T. Madanbashi, K. Sugiura, R. Clérac, and H. Nojiri, Inorg. Chem. **44**, 6969 (2005); D. Li, S. Parkin, G. Wang, G. T. Yee, R. Clérac, W. Wernsdorfer, and S. M. Holmes, J. Am. Chem. Soc. **128**, 4214 (2006); T. Glaser, M. Heidemeier, T. Weyhermüller, R.-D. Hoffmann, H. Rupp, and P. Müller, Angew. Chem., Int. Ed. **45**, 6033 (2006); J. M. Zadrozny, D. E. Freedman, D. M. Jenkins, T. D. Harris, A. T. Iavarone, C. Mathonière, R. Clérac, and J. R. Long, Inorg. Chem. **49**, 8886 (2010); Y.-Z. Zhang, B.-W. Wang, O. Sato, and S. Gao, Chem. Commun. **46**, 6959 (2010).

[7] C. Zener, Phys. Rev. **82**, 403 (1951); P. W. Anderson and H. Hasegawa, Phys. Rev. **100**, 675 (1955).

[8] M. B. Robin and P. Day, Adv. Inorg. Chem. Radiochem. **10**, 247 (1967).

[9] G. C. Allen and N. S. Hush, Prog. Inorg. Chem. **8**, 357 (1967); N. S. Hush, Prog. Inorg. Chem. **8**, 391 (1967).

[10] C. Creutz and H. Taube, J. Am. Chem. Soc. **95**, 1086 (1973); D. O. Cowan, C. LeVanda, J. Park, and F. Kaufman, Acc. Chem. Res. **6**, 1 (1973).

[11] G. Blondin and J.-J. Girerd, Chem. Rev. **90**, 1359 (1990).

[12] X.-Q. Ding, E. L. Bominaar, E. Bill, H. Winkler, A. X. Trautwein, S. Drüeke, P. Chaudhuri, and K. Wieghardt, J. Chem. Phys. **92**, 178 (1990).

[13] D. R. Gamelin, E. L. Bominaar, M. L. Kirk, K. Wieghardt, and E. J. Solomon, J. Am. Chem. Soc. **118**, 8085 (1996).

[14] B. Bechlars, D. M. D'Alessandro, D. M. Jenkins, A. T. Iavarone, S. D. Glover, C. P. Kubiak, and J. R. Long, Nat. Chem. **3**, 362 (2010).

[15] D. A. Garanin and E. M. Chudnovsky, Phys. Rev. B **56**, 11102 (1997); M. N. Leuenberger and D. Loss, Nature (London) **410**, 789 (2001); M. H. Jo, J. E. Grose, K. Baheti, M. M. Deshmukh, J. J. Sokol, E. M. Rumberger,

D. N. Hendrickson, J. R. Long, H. Park, and D. C. Ralph, Nano Lett. **6**, 2014 (2006); A. Ardavan, O. Rival, J. J. L. Morton, S. J. Blundell, A. M. Tyryshkin, G. A. Timco, and R. E. P. Winpenny, Phys. Rev. Lett. **98**, 057201 (2007); L. Bogani and W. Wernsdorfer, Nat. Mater. **7**, 179 (2008); P. C. E. Stamp and A. Gaita-Arino, J. Mater. Chem. **19**, 1718 (2009); M. Mannini, F. Pineider, P. Sainctavit, C. Danieli, E. Otero, C. Sciancalepore, A. M. Talarico, M. A. Arrio, A. Cornia, D. Gatteschi, and R. Sessoli, Nat. Mater. **8**, 194 (2009); S. Loth, K. von Bergmann, M. Ternes, A. F. Otte, C. P. Lutz, and A. J. Heinrich, Nat. Phys. **6**, 340 (2010).

[16] J. Woodward, Phil. Trans. Roy. Soc. London, **33**, 15 (1724).

[17] W. Kaim and G. K. Lahiri, Angew. Chem. Int. Ed. Engl. **46**, 1778 (2007); K. Demadis, C. M. Hartshorn, and T. J. Meyer, Chem. Rev. **101**, 2655 (2001); W. Kaim, A. Klein, and M. Glöckle, Acc. Chem. Res. **33**, 755 (2000); D. M. D'Alessandro and F. R. Keene, Chem. Rev. **106**, 2270 (2006); D. M. D'Alessandro and F. R. Keene, Chem. Soc. Rev. **35**, 424 (2006); B. S. Brunschwig, C. Creutz, and N. Sutin, Chem. Soc. Rev. **31**, 168 (2002).

[18] A. S. Borovik, V. Papaefthymiou, L. F. Taylor, O. P. Anderson, and L. Que, Jr., J. Am. Chem. Soc. **111**, 6183 (1989) and references therein; M. Suzuki, H. Oshio, A. Uehara, K. Endo, M. Yanaga, S. Kida, and K. Saito, Bull. Chem. Soc. Jpn. **61**, 3907 (1988) and references therein; M. S. Mashuta, R. J. Webb, K. J. Oberhausen, J. F. Richardson, R. M. Buchanan, and D. N. Hendrickson, J. Am. Chem. Soc. **111**, 2745 (1989); A. S. Borovik, B. P. Murch, L. Que, Jr., V. Papaefthymiou, and E. Munck, *ibid.* **109**, 7190 (1987); B. S. Snyder, G. S. Patterson, A. J. Abrahamson, and R. H. Holm, *ibid.* **111**, 5214 (1989); H. G. Jang, S. J. Geib, Y. Kaneko, M. Nakano, M. Sorai, A. L. Rheingold, B. Montez, and D. N. Hendrickson, *ibid.* **111**, 173 (1989).

[19] S. K. Dutta, J. Ensling, R. Werner, U. Flörke, W. Haase, P. Gütlich, and K. Nag, Angew. Chem. Int. Ed. **36**, 152 (1997); S. Drüeke, P. Chaudhuri, K. Pohl, K. Wieghardt, X.-Q. Ding, E. Bill, A. Sawaryn, A. X. Trautwein, H. Winkler, and S. J. Gurman, J. Chem. Soc., Chem. Commun. 59 (1989); D. Lee, C. Krebs, B. H. Huynh, M. P. Hendrich, and S. J. Lippard, J. Am. Chem. Soc. **122**, 5000 (2000); L. O. Spreer, A. Li, D. B. MacQueen, C. B. Allan, J. W. Otvos, M. Calvin, R. B. Frankel, and G. C. Papaefthymiou, Inorg. Chem. **33**, 1753 (1994).

[20] X.-Q. Ding, E. Bill, A. X. Trautwein, H. Winkler, A. Kostikas, V. Papaefthymiou, A. Simopoulos, P. Beardwood, and J. F. Gibson, J. Chem. Phys. **99**, 6421 (1993).

[21] M. Stebler, A. Ludi, and H.-B. Burgi, Inorg. Chem. **25**, 4743 (1986).

[22] H. R. Chang, S. K. Larsen, P. D. W. Boyd, C. G. Pierpont, and D. N. Hendrickson, J. Am. Chem. Soc. **110**, 4565 (1988); B. F. Hoskins, R. Robson, and G. A. Williams, Inorg. Chim. Acta **16**, 121 (1976); *The Cambridge Crystallographic Database (CSD) Systems*, Version 5.30, November 2008.

[23] D. D. LeCloux, R. Davydov, and S. J. Lippard, J. Am. Chem. Soc. **120**, 6810 (1998).

[24] R. R. Gagné, C. L. Spiro, T. J. Smith, C. A. Hamann, W. R. Thies, and A. D. Shiemke, J. Am. Chem. Soc. **103**, 4073 (1981).

[25] L. Que, Jr. and A. E. True, Prog. Inorg. Chem. **38**, 97 (1990).

[26] V. Papaefthymiou, J.-J. Girerd, I. Moura, J. J. G. Moura, and E. Münck, J. Am. Chem. Soc. **109**, 4703 (1987); L. Noodleman and D. A. Case, Adv. Inorg. Chem. **38**, 423 (1992); B. R. Crouse, J. Meyer, and M. K. Johnson, J. Am. Chem. Soc. **117**, 9612 (1995).

[27] E. Münck and E. L. Bominaar, Science **321**, 1452 (2008).

[28] H. Andres, E. L. Bominaar, J. M. Smith, N. A. Eckert, P. L. Holland, and E. Münck, J. Am. Chem. Soc. **124**, 3012 (2002).

[29] E. L. Bominaar, Z. Hu, E. Münck, J.-J. Girerd, and S. A. Borshch, J. Am. Chem. Soc. **117**, 6976 (1995).

[30] Z. Otwinowski and W. Minor, Methods Enzymol. **276**, 307 (1997); V. N. Sonar, M. Venkatraj, S. Parkin, and P. A. Crooks, Acta Cryst. C **63**, o493 (2007).

[31] G. M. Sheldrick, SHELXL-97, Crystal Structure Refinement Program, University of Göttingen, 1997.

[32] See supplementary material at http://dx.doi.org/10.1063/1.3581028 for crystallographic information files, obtained at 120 and 293 K, for [$Fe_2L(\mu$-OAc)2]ClO4, **1**, detailed information concerning the magnetic and Mössbauer analysis, Tables S1 to S5, and Figs. S1 to S9.

[33] S. Mohanta, K. K. Nanda, L. K. Thompson, U. Flörke, and K. Nag, Inorg. Chem. **37**, 1465 (1998).

[34] O. Kahn, *Molecular Magnetism* (Wiley, New York, 1993).

[35] C. Saal, S. Mohanta, K. Nag, S. K. Dutta, R. Werner, W. Haase, E. Duin, and M. K. Johnson, Ber. Bunsenges. Phys. Chem. **100**, 2086 (1996).

[36] S. M. Ostrovsky, R. Werner, K. Nag, and W. Haase, Chem. Phys. Lett. **320**, 295 (2000).

[37] In a private communication, the authors of Ref. 35 have indicated that x_P is the fractional amount of impurity included in the fit of the effective magnetic moment of **2**.

[38] G. Pen, J. van Elp, H. Jang, L. Que, Jr., W. H. Armstrong, and S. P. Cramer, J. Am. Chem. Soc. **117**, 2515 (1995); M. J. Knapp, J. Krzystel, L.-C. Brunel, and D. N. Hendrickson, Inorg. Chem. **38**, 3321 (1999); J. R. Hagadorn, L. Que, Jr., W. B. Tolman, I. Prisecaru, and E. Münck, J. Am. Chem. Soc. **121**, 9760 (1999).

[39] M. P. Shores, J. J. Sokol, and J. R. Long, J. Am. Chem. Soc. **124**, 2279 (2002).

[40] E. Buluggiu and A. Vera, Z. Naturforsch. **31a**, 911 (1976).

[41] K. S. Cole and R. H. Cole, J. Chem. Phys. **9**, 341 (1941); C. J. F. Boettcher, *Theory of Electric Polarisation* (Elsevier, Amsterdam, 1952); S. M. Aubin, Z. Sun, L. Pardi, J. Krzystek, K. Folting, L.-J. Brunel, A. L. Rheingold, G. Christou, and D. N. Hendrickson, Inorg. Chem. **38**, 5329 (1999).

[42] E. Bill, F.-H. Bernhardt, A. X. Trautwein, and H. Winkler, Eur. J. Biochem. **147**, 177 (1985).

[43] P. Gütlich, R. Link, and A. X. Trautwein, *Mössbauer Spectroscopy in Tansition Metal Chemistry* (Springer, Heidelberg, 1978).

[44] S. C. Bhargava, J. E. Knudsen, and S. Mørup, J. Phys. C **12**, 2879 (1979).

[45] M. Blume, Phys. Rev. Lett. **18**, 305 (1967).

[46] H. Winkler, E. Bill, A. X. Trautwein, A. Kostikas, A. Simopoulos, and A. Terzis, J. Chem. Phys. **89**, 732 (1988).

[47] L. Chianchi, F. Del Giallo, G. Spina, W. Reiff, and A. Caneschi, Phys. Rev. B **65**, 064415 (2002).

[48] S. Dattagupta and M. Blume, Phys. Rev. B **10**, 4540 (1974).

[49] G. K. Shenoy, F. E. Wagner, and G. M. Kalvius, in *Mössbauer Isomer Shifts*, edited by G. K. Shenoy and F. E. Wagner (North-Holland, Amsterdam, 1978), p. 49.

[50] T. Owen, F. Grandjean, G. J. Long, K. V. Domasevitch, and N. Gerasimchuk, Inorg. Chem. **47**, 8704 (2008).